Cognitive inhibition of number/length interference in a Piaget-like task in young adults: evidence from ERPs and fMRI.

Gaëlle Leroux, Marc Joliot, Stéphanie Dubal, Bernard Mazoyer, Nathalie Tzourio-Mazoyer, Olivier Houdé

Cognitive inhibition of number/length interference in a Piaget-like task in young adults: Evidence from ERPs and fMRI

Gaëlle Leroux[1], Marc Joliot[1], Stéphanie Dubal[3], Bernard Mazoyer[1, 2], Nathalie Tzourio-Mazoyer[1], and Olivier Houdé[1, 2].

1 Groupe d'Imagerie Neurofonctionnelle (GIN), UMR 6194, CNRS, CEA, Universités de Caen et Paris-5, France.
2 Institut Universitaire de France (IUF).
3 Vulnérabilité, Adaptation et Psychopathologie, UMR 7593, CNRS, Université Paris-6, France.

Contract grant sponsors: CEA/Région Basse Normandie, France, and ACI "Neurosciences intégratives et computationnelles" from the French Ministry of Research.

Correspondence to: Dr Marc Joliot, Groupe d'Imagerie Neurofonctionnelle (GIN), UMR 6194, CNRS, CEA, Universités de Caen et Paris-5, GIP Cyceron, BP 5229, 14074 Caen Cedex, France.
E-mail: joliot@cyceron.fr

Part of the results was presented during the 10th Annual Meeting of the Organization for Human Brain Mapping in Budapest, Hungary (2004).

Abstract: 249 words.

Abstract

We sought to determine whether the neural traces of a previous cognitive developmental stage could be evidenced in young adults. In order to do so, twelve young adults underwent two functional imaging acquisitions (EEG then fMRI). During each session, two experimental conditions were applied: a Piaget-like task with number/length interference (INT), and a reference task with number/length covariation (COV). To succeed at Piaget's numerical task, which children under the age of seven usually fail, the subjects had to inhibit a misleading strategy, namely the visuospatial length-equals-number bias, a quantification heuristic that is often relevant and that continues to be used through adulthood.

Behavioral data confirmed that although there was an automation in the young adult subjects as assessed by the very high number of accurate responses (>97%), the inhibition of the "length equals number strategy" had a cognitive cost, as the reaction times were significantly higher in INT than in COV (with a difference of 230 msec).

The event-related potential results acquired during the first session showed electrophysiological markers of the cognitive inhibition of the number/length interference. Indeed, the frontal N2 was greater during INT than during COV, and a $P3_{late}$/P6 was detected only during INT.

During the fMRI session, a greater activation of unimodal areas (the right middle and superior occipital cortex), and in the ventral route (the left inferior temporal cortex) was observed in INT than in COV. These results seem to indicate that when fully automated in adults, inhibition processes might take place in unimodal areas.

Key words: Piaget-like task, number, visuospatial interference, inhibition, Event-Related Potential (ERP), functional Magnetic Resonance Imaging (fMRI).

Introduction

In the study of human evolution to Homo sapiens, as well as in the study of cognitive development, the inhibition of misleading strategies is regarded today as a crucial mechanism of adaptation, a possible "Darwinian algorithm" [Dempster 1995; Diamond 1991; Diamond et al., 2002; Houdé 2000; Houdé and Tzourio-Mazoyer 2003; Houdé et al., 2000]. It is an executive process involved in attention, self-regulation, and consciousness [Posner and Rothbart 1998]. In cognitive developmental psychology, a very famous inhibition task is Piaget's numerical task [Dempster 1995; Houdé 2000; Houdé and Guichart 2001; Piaget 1952]. When shown two rows of objects containing the same number of objects but having different lengths (because the objects in one of the rows have been spread apart), the child has to say whether the two rows have the same number of objects. Until the age of seven, children usually erroneously say there are more objects in the longer row. To succeed in this cognitive task, children have to inhibit a misleading strategy, namely the visuospatial length-equals-number bias [Houdé 2000; Houdé and Guichart 2001], an often-relevant quantification heuristic still used by adults.

In a previous Event-Related Potential (ERP) study [Daurignac et al., 2005] we found, in adults, electrophysiological correlates (namely an increased N2 amplitude) reflecting the inhibition of the numerical visuospatial bias in Piaget's numerical task. For accuracy in numerical quantification, the adult brain still has to control childlike cognition biases that are stored in a kind of “developmental memory”. It is known in cognitive developmental neuroscience that the acquisition of a fully coordinated and controlled set of executive functions (namely, response inhibition) occurs relatively late in brain development [Keating 2004; Paus 2005; Steinberg 2005].

In this study our objective was both to replicate our previous ERP results in Piaget's numerical task and to use functional magnetic resonance imaging (fMRI) to explore the

- 3 -

neural networks that young adults recruit to resolve this developmental task. To this aim, we used two experimental conditions: a Piaget-like task with number/length interference and a reference task with number/length covariation.

Materials and methods

Subjects

Twelve healthy volunteers (7 men), aged 23 ± 3 years, all right-handed as evaluated by the Edinburgh Inventory [Oldfield 1971], participated in this study. They were free from cerebral abnormality as assessed by the T1-weighted magnetic resonance images of their brain. They had normal vision without correction. All gave their informed written consent to the study, which was accepted by our local ethics committee.

Stimuli

The stimuli used in this study were identical to those previously used in our group by Houdé and Guichart [Houdé and Guichart 2001]. An item was displayed on a computer screen divided in two by a horizontal line (see Fig. 1). On each side of the line there was a row of shapes (blue, cyan, green, red, and yellow squares or rectangles). The two rows could be of equal or different sizes (one to four shapes), and the subject had to judge their numerical equivalence. They were instructed to respond by pressing the "same-number" button or the "not-the-same-number" button as quickly as possible, without making any errors (the side of the response, using the right and the left hand, was counterbalanced in half of the subjects). When a button was pressed, the computer recorded the subject's reaction time (RT) (measured in milliseconds since stimulus onset). Two kinds of displays were set up, one called "covariation" (COV) and the other one "interference" (INT). In COV displays, the number of objects and the row length covaried (see the left screen in

Fig. 1), while in INT displays, the shapes in one of the rows were spread apart, and thus involved number/length interference (see the right screen in Fig. 1). This latter kind of display corresponds to a Piaget-like task.

---------- Include Figure 1 about here ----------

Since in COV displays, the subjects had – by definition –to always respond by pressing the "not-the-same-number" button, while in INT displays they had to press the "same-number" button, it was important to overcome any strategy consisting in a systematic answer. We therefore introduced 20% of displays with "same-number" responses in COV and "not-the-same-number" responses in INT.

Task design

Each subject was tested in two sessions on one day. In the first session, in the morning, we recorded electroencephalograms (EEGs) during two runs: COV, then INT. In the second session, in the afternoon, we measured brain activity during the same displays with functional magnetic resonance imaging (fMRI).

In the EEG session, each run was composed of 100 stimuli and they subtended a vertical visual angle of 1.1° and a horizontal visual angle of 1.3°. They were projected on a centered screen by an optical system with mirrors (the display was controlled by a computer running in MS-DOS mode). The inter-stimulus interval (ISI) was 2700 ± 75 msec. A gray screen was displayed before each new stimulus (even if the button response was not pressed) in order to avoid blinks during the baseline period. Before the first run, all subjects performed familiarization trials with COV stimuli (a maximum of 10).

In the fMRI session, the stimulus displays were strictly the same than the EEG session. Each fMRI run was composed of 6 blocks of 8 COV or INT stimuli, alternating with 24-sec cross-fixation periods. The ISI was 3000 ± 80 msec. Subjects viewed a backlit

projection (STIM software, NeuroScan Inc., El Paso, TX, USA) from within the magnet bore through a mirror mounted on the head coil.

ERP data acquisition and analysis

Scalp voltages were recorded with a cap (FMS) of 64 Ag/AgCl electrodes. A medium or a large cap was chosen accordingly to the subject's head size. The Cz location was placed on the vertex of the head (10-20 system) and the other midline electrodes on the mid-sagittal plane. For one subject, the scalp voltages were not recorded for technical reasons. The electrode impedance was maintained below 10 KΩ. The reference electrodes consisted of two linked-earlobe references with a shoulder ground. The electro-oculogram (EOG) was monitored with two right supra-orbital and infra-orbital electrodes (vertical EOG) and two electrodes on the external canthi (horizontal EOG). The electric signals were recorded using CTF amplifiers (64 EEG and 2 EOG channels, low-pass 100 Hz) and digitalized (sampling rate 625 Hz). The scalp voltages between -0.4 sec (pre-stimuli) and +1.7 sec (post-stimuli) of the onset of each stimulus were recorded with a total of 100 trials per condition.

EEG data were processed offline in three stages using the CTF software package (Coquitlam, Canada), EEGLAB v4.4 [Delorme and Makeig 2004] and in-house software.

In the first stage, an artifact-handling procedure was implemented in two steps including a global correction and trial-based manual rejections. For the global correction, we used a method based on independent component analysis decomposition as described by Jung et al. [Jung et al., 2000]. This phase was followed by a visual inspection of the individual trials to exclude those showing artifacts (above 100 µV peak-to-peak or high alpha contaminations). On average, the percentage of epochs removed was around 4% (SD 3%, N = 22) per run and no difference was found between the two conditions.

- 6 -

In the second stage, only artifact free and correctly answered trials were included in the individual average ERPs: 94% of the acquired trials for the Covariation ERPs (SD 2.4%, minimum of 92%, N = 11 subjects) and 88% for the Interference ERPs (SD 3.6%, minimum of 82%, N = 11 subjects). The average ERPs were band-pass filtered (0.6 Hz – 30 Hz) with a 200 msec pre-stimuli baseline.

In the last stage of the processing, we identified, in each subject, three distinct components in the Covariation ERPs (i.e. N1, N2, and $P3_{early}$), and four components in the Interference ERPs (i.e. N1, N2, $P3_{early}$, and $P3_{late}$). For each component, the latencies and the amplitudes were measured for different subsets of electrodes. The N1 was measured at the back of the brain with the parietal and occipital electrodes (N = 29), the N2 in the frontal region up to the vertex (N = 33), and both $P3_{early}$ and $P3_{late}$ with a set symmetrically placed around the vertex (N = 50). The average amplitude and the average latency of each component were computed for each condition (COV and INT) from the ten individual values (another subject was excluded at the last stage of the analyses because we were unable to unequivocally identify his N2 component). Maximum individual voltages were assessed in four time windows (individually adjusted), corresponding roughly to N1 (100 msec to 200 msec), N2 (200 msec to 300 msec), a $P3_{early}$ (300 msec to 400 msec) and a $P3_{late}$ (400 msec to 600 msec).

For the N1, the N2 and the $P3_{early}$ components, statistical comparisons for electrophysiological parameters (amplitude and latency) were computed by separated repeated-measure analyses of variance (ANOVAs) with two within-subject variables: conditions (COV, INT) and electrode sites (29 for the N1, 33 for the N2, and 50 for the $P3_{early}$). Greenhouse-Geisser corrections were applied when appropriate.

- 7 -

fMRI data acquisition and analysis

MRI acquisitions were conducted on a GE Signa 1.5-Tesla Horizon Echospeed scanner (General Electric, BUC, France). The session started with two anatomical acquisitions. First, a high-resolution structural T1-weighted sequence (T1-MRI) was acquired using a spoiled gradient recalled sequence (SPGR-3D, FOV = 240 x 240 x 186 mm^3, sampling = 0.94 x 0.94 x 1.5 mm^3) to provide detailed anatomic images and to define the location of the 21 axial slices to be acquired during both the second anatomical acquisition and the functional sequences. Note that, because of the limited size of the field of view, the cerebellum was usually not imaged. The second anatomical acquisition consisted in a double echo proton density / T2-weighted (PD-MRI / T2-MRI) sequence (FOV = 240 x 240 x 105 mm^3, sampling = 0.94 x 0.94 x 5 mm^3). Each of the two following functional runs (COV and INT) consisted in a time series of 110 EPI volumes (TR = 3 sec, TE = 60 msec, FA = 90°, sampling = 3.75 x 3.75 x 5mm^3). To ensure the signal stabilization, the first three EPI volumes were discarded at the beginning of each run.

The pre-processing was built on the basis of SPM99b subroutines [Ashburner and Friston 1999; Friston et al., 1995], AIR5.0 [Woods et al., 1992], Atomia [Verard et al., 1997] and locally developed ones encapsulated in a semi-automatic processing pipeline. The pre-processing included 9 steps: (1) correction for differences in EPI image acquisition time between slices, (2) rigid spatial registration of each of the EPI volumes onto the fourth EPI volume (EPI4) of the first acquired run, (3) computation of the spatial rigid registration and re-sampling matrices from EPI4 to T2-MRI and DP-MRI to T1-MRI, (4) computation of the nonlinear registration matrix for stereotaxic normalization of the T1-MRI on the Montreal Neurological Institute T1-weighted templates T1-MNI, [Collins et al., 1994] (SPM99b stereotaxic normalization with 12-parameter rigid body

transformations and 7 x 8 x 7 nonlinear basis functions, 12 nonlinear iterations, medium regularization, bounding box in between -90 to +91 mm left-right, -126 to +91 mm back-front and -72 to +109 mm feet-head directions, sampling 2 x 2 x 2 mm^3), (5) combination of the matrices computed at the previous two steps, visual checking, and optional optimization of the EPI4 to T1-MNI registration in the stereotaxic space, (6) spatial resampling of each EPI volume into the T1-MNI stereotaxic space, (7) spatial smoothing of each EPI volume by a Gaussian filter (FWHM = 8 x 8 x 8 mm^3), (8) high-pass filtering (cut-off of 0.0102 Hz) of each voxel time course, and (9) normalization of the voxel values by the average of its value in the course of the two runs (i.e. across time course).

For the fMRI data processing, the region-of-interest analysis was based on the anatomical region-of-interest (AROI) parcellation of the single T1 subject MNI MRI brain data [Tzourio-Mazoyer et al., 2002]. The selected bilateral AROIs belonged to the occipital and the ventral temporal cortex, as our tasks were presented visually and involved both ventral and dorsal visual pathways [Gulyas et al., 1994; Haxby et al., 1991; Vidnyanszky et al., 2000; Zeki et al., 1991], the right parietal cortex since the tasks required the dorsal pathway recruitment and attention [Corbetta et al., 1993; Petit et al., 1996], the left parietal cortex since the tasks involved a numerical decision [Chochon et al., 1999; Piazza et al., 2002; Zago et al., 2001], and the lateral and medial frontal cortex and cingulates because the tasks concerned executive functions, namely conflict monitoring and inhibition [Bush et al., 2000; Bush et al., 2002; Houdé and Tzourio-Mazoyer 2003; Houdé et al., 2001], leading to a subset of 19 AROIs for each hemisphere. For each of the subjects, each of the selected AROIs and each run (COV and INT), an average BOLD-signal temporal course was computed. Note that the analysis field of view (common to all subjects) was defined between z = -19 mm and z = +60 mm.

- 9 -

Statistical analysis of fMRI data

The first statistical analysis, named the *conjunction* analysis, highlighted the regions that were activated or deactivated respectively in both conditions. Using the COV time courses, we computed for each AROI and each subject the signal variation of the task periods *minus* the average signal of the cross fixation periods. The task signals were defined in the interval between 3 sec and 24 sec after each block onset and the fixation signals during the 9 sec before each block onset. The values of each AROI were subjected to a unilateral Student's t-test. The same analysis was conducted on the INT data. We reported the regions that survived a 0.05 (uncorrected) p-value threshold in both conditions (COV and INT).

In the second statistical analysis, named *overall condition effect* analysis, a repeated-measure ANOVA was performed in order to test effects between two within-subject variables: conditions (COV, INT) and hemodynamic response latency (8 HRLs). The HRLs were sampled every 3 sec in the interval between 3 sec and 24 sec (8 samples) following each block onset (contrasted to the fixation signal period, see above). Regions surviving the statistical threshold of 0.05 (uncorrected) for each overall effect (condition, HRL) and the condition x HRL interaction were reported.

Since this study is the first to explore the neural networks of the inhibition of a number/length interference with fMRI in a Piaget-like task in adults, we chose an uncorrected exploratory statistical threshold of 0.05 to detect the significant AROIs.

Results

Below we present the behavioral data, reaction times and error rate, followed by the electrophysiological (ERPs) and hemodynamic (fMRI) imaging data in the two

- 10 -

experimental conditions: number/length interference (INT) and number/length covariation (COV).

Behavioral data

Reaction times. Only the reaction times (RTs) for the accurate responses were considered (>97%). A repeated-measure ANOVA was computed on RTs with two within-subject variables: conditions (COV, INT) and sessions (EEG, fMRI). It revealed a significant overall condition effect, as the average RT was longer for INT (785 ± 83 msec) than for COV (555 ± 103 msec) [$F(1, 11) = 229.18$, $P < .0001$]. The results also indicated that neither the session overall effect nor the interaction was significant.

---------- Include Figure 2 about here ----------

In order to test habituation during the EEG session, RTs were artificially segregated in blocks of 8 stimuli (as they were during the fMRI session) and the block averages (11) were computed (see Fig. 2, top part). A repeated-measure ANOVA with condition (COV, INT) and block as within-subject variables confirmed the previous condition overall effect [$F(1,11) = 116.75$, $P < 0.0001$]. It also showed a habituation effect through the 11 blocks for both conditions, COV then INT [$F(10,110) = 23.39$, $P < 0.0001$], with the strongest decrease in RTs in the first two blocks as attested by a post-hoc Fischer's test ($P < 0.0001$). A significant interaction effect indicated that this habituation was sharper in INT than in COV [$F(10, 110) = 6.01$, $P < 0.0001$].

In order to test habituation during the fMRI session, we similarly computed a repeated-measure ANOVA on RTs with condition (COV, INT) and block (6) as within-subject variables. It confirmed the condition overall effect [$F(1, 11) = 41.03$, $P < 0.0001$] and also the habituation effect through the 6 blocks for both conditions, COV then INT [$F(5, 55) = 29.15$, $P < 0.0001$], with the strongest decrease in RTs in the first three blocks as

- 11 -

attested by post-hoc Fischer's tests ($P < 0.0001$ and $P = 0.0160$ respectively). This habituation effect was not different in INT and in COV, the interaction not being significant.

We also controlled the motor response lateralization effect on RTs. Whatever the experimental condition (INT or COV) and the session (EEG or fMRI), no significant effect was observed.

Error rates. The general average error rate was less than 3% (including 1.7% non-responses). A repeated-measure ANOVA was computed on error percentages with two within-subject variables: conditions (COV, INT) and sessions (EEG, fMRI) (see Fig. 2, bottom part). It revealed a significant overall condition effect, as the average error percentage was higher for INT (3.5%) than for COV (0.7%) [$F(1, 11) = 16.15$, $P = 0.002$]. The results also indicated a significant overall session effect characterized by a decrease in error rate between the two sessions [$F(1, 11) = 20.80$, $P = 0.0008$], especially in the INT condition [interaction effect: $F(1, 11) = 17.44$, $P = 0.0015$].

For the EEG session, error percentages were artificially segregated in blocks of 8 stimuli (as they were during the fMRI session) and the block averages (11) were computed. A repeated-measure ANOVA with condition (COV, INT) and block as within-subject variables confirmed the previous condition overall effect [$F(1, 11) = 18.04$, $P = 0.0014$]. It also showed a habituation effect through the 11 blocks for both conditions, COV then INT [$F(10,110) = 8.16$, $P < 0.0001$], with the strongest decrease in errors in the first two blocks as attested by a post-hoc Fischer's test ($P < .0001$). A significant interaction effect indicated that this habituation was mainly observed in INT [$F(10, 110) = 7.71$, $P < 0.0001$].

- 12 -

Note that the repeated-measure ANOVA on fMRI error percentages was impossible because the subjects committed too few errors (variance was not computable for some blocks). The average error rate was exactly the same in INT and in COV (0.5%).

ERP data

Fig. 3 illustrates the grand average waveforms from the covariation (COV) and the interference (INT) conditions at midline locations, for the N1, N2, $P3_{early}$, and $P3_{late}$ components. Fig. 4 illustrates their relative topographic maps, while Table I summarizes the main results of the Student's tests (condition and electrode effects) on their amplitudes and latencies.

---------- Include Figure 3 about here ----------

N1 component. A first negative deflection peaking at 146 and 149 msec (COV and INT, respectively) was identified as the N1 component. Only an electrode effect was observed in amplitude, supporting the customary occipital topography of N1 (the greatest effects were observed at the bilateral occipital and parieto-occipital electrodes).

---------- Include Table I about here ----------

N2 component. A second negative deflection peaking at 260 and 277 msec (COV and INT, respectively) was identified as the N2 component. N2 amplitude and latency were significantly larger and longer in INT than in COV (condition effects) and an electrode effect on amplitude supported the fronto-central distribution (the greatest effects were observed at the Fz and AFz electrodes).

$P3_{early}$ component. A positive deflection peaking at 359 and 369 msec (COV and INT respectively) was identified as the $P3_{early}$ component. A $P3_{early}$ condition effect was significantly detected in amplitude, and an electrode effect was observed in amplitude supporting a centro-parietal distribution (the greatest effects were observed at the C2, Cpz, and Cz electrodes).

- 13 -

$P3_{late}$ component. Finally, a positive deflection peaking at 556 msec was only identified as a $P3_{late}$ in INT. For this reason, no statistical comparison was possible between the two conditions. However, an electrode effect was observed, which supported the centro-parietal distribution (the greatest effects were also observed at the CP_z, CZ, and C2 electrodes for INT).

---------- Include Figure 4 about here ----------

fMRI data

The fMRI data presented below are analyzed in three ways (see Table II): (1) the conjunction analysis (areas activated in both conditions, INT and COV), (2) the overall condition effect, and (3) the percentage change of the block response shape depending on the experimental conditions (condition x HRL interaction).

Conjunction analysis: areas activated in both conditions. This analysis shed light on a bilateral posterior network including primary (V1) and associative areas of ventral and dorsal pathways (see Fig. 5). The visual areas of the ventral pathway were extended as far as V4 (the lingual and the fusiform gyri); on the right hemisphere, the occipito-temporal junction was also activated (the posterior part of the inferior temporal gyrus). The areas of the dorsal pathway included the middle and superior occipital gyri, with an internal activation of the cuneus, as well as the inferior and superior parietal cortex.
Finally, the conjunction highlighted a set of right frontal areas on the external surface: the middle frontal gyrus and the opercular part of the inferior frontal gyrus.

---------- Include Figure 5 about here ----------

Overall condition effect. This analysis implicated regions according to three patterns of activity: (1) the regions that were more activated in the interference condition (INT) than in covariation (COV) (see Fig. 6), (2) the regions that were deactivated during INT

- 14 -

and activated in COV (see Fig. 7, blue regions) and (3) the regions that were more activated in COV than in INT (see Fig. 7, yellow regions).

The regions that were more activated in INT than in COV were the right middle and superior occipital cortex, and the posterior part of the left inferior temporal gyrus.

---------- Include Figure 6 about here ----------

Among the regions that were deactivated in INT and activated in COV, we first noticed the bilateral anterior cingulate, the orbital part of the left superior medial frontal gyrus, the bilateral superior medial frontal gyrus, the left middle and superior frontal gyri, and the orbital part of the left inferior frontal gyrus. Finally, we noticed the left middle temporal gyrus and the left supramarginalis gyrus (SMG).

The regions that were more activated in COV than in INT were the bilateral median cingulate and the right middle temporal gyrus.

---------- Include Figure 7 about here ----------

Percentage change of the block response shape depending on the experimental conditions. This analysis shed light on different activation/deactivation patterns. In the first one, we observed a greater activation in INT than in COV in the left inferior occipital cortex. In another pattern, we observed a greater activation in COV than in INT at the beginning of the block, whereas at the end of the block, the opposite occurred: activation was greater in INT than in COV. The regions with activity fitting this pattern were the left superior occipital cortex, the left superior parietal cortex, and the right inferior temporal cortex.

Eventually, two other patterns were observed: a greater activation in COV than in INT (the left lingual gyrus, the left cuneus, the right SMG, and the right middle temporal gyrus) and an activation in COV with deactivation in INT (the right superior temporal gyrus and the left SMG).

- 15 -

Discussion

Behavioral data

The behavioral data indicated longer RTs for the accurate responses (>97%) in the interference condition (INT) than in the covariation condition (COV) in both sessions (EEG, fMRI), with no difference between the two sessions. This result corresponds to a classical interference effect [Houdé 2001]. Recall that in INT there was number/length interference and that the subjects should therefore inhibit the misleading strategy "length equals number" to reach a correct answer. This strategy inhibition triggers, longer RTs in INT than in COV (where number and length covaried) in adults, as it does in children [Houdé and Guichart 2001]. In addition, the results showed a decrease in RTs within both sessions and in both conditions, that corresponded to a classical habituation effect.

The behavioral data also indicated that the mean error rate in the numerical judgments was very low in both conditions, which was expected, as it was known that this child-psychology task can be successfully performed by children as young as seven years old [Houdé and Guichart 2001; Piaget 1952]. Nevertheless, the specific large decrease in error rate in the first two INT blocks (in the EEG session) is congruent with the strongest RT habituation effect during the same blocks. It confirms that in this case, contrary to COV, the subjects had to inhibit the usual strategy "length equals number" for the first time. Note that during cognitive development, the Piaget-like (INT) task is also successfully solved later (at seven years of age) than the number/length covariation task (COV), which preschoolers are able to solve.

Thus, the behavioral data confirm that INT was a task that required strong cognitive inhibition by the subjects and that COV was a reference task.

- 16 -

ERP data

The first difference in ERP was observed for the N2 component over the fronto-central area, of which the amplitude and latency were significantly larger and longer in INT than in COV. The amplitude result is consistent with our previous work using similar experimental stimuli [Daurignac et al., 2005]. In this study, the amplitude of the N2 was also enhanced after stimuli with number/length interference. We interpreted this as an increase of the energetic cost in information processing when the heuristic "length equals number" strategy had to be inhibited. A greater N2 component is known to be involved in the NoGo condition (where the subjects had to inhibit a response) of different Go/NoGo designs [Bekker et al., 2005; Bruin et al., 2001; Eimer 1993; Falkenstein et al., 1999; Jackson et al., 1999; Lavric et al., 2004; Nieuwenhuis et al., 2004; Nieuwenhuis et al., 2003].

The $P3_{early}$ component over the centro-parietal areas was also significantly larger (in amplitude) in COV than in INT, while the inter-condition difference in latencies was not significant. This amplitude difference is consistent with Go/NoGo data showing a larger P3 during the Go condition than during the NoGo condition (inhibition condition) [Bruin et al., 2001; Eimer 1993; Falkenstein et al., 1995; Hunter et al., 2001; Jackson et al., 1999; Katayama and Polich 1998; Kopp et al., 1996; Linden et al., 1999]. It is also consistent with oddball paradigm studies showing a larger P3 for target stimuli than for nontarget stimuli (inhibition condition) [Hunter et al., 2001; Katayama and Polich 1998; Linden et al., 1999].

Finally, an additional component over the centro-parietal area, called $P3_{late}$, was only observed in INT. This component, peaking around 500-600 msec, could be related to nontarget stimuli (inhibition condition) during three-stimulus paradigms (target, nontarget, and standard) [Comerchero and Polich 1998; 1999; Knight and Scabini 1998; Polich 2003;

2004; Polich and Comerchero 2003]. More generally, this second positivity ($P3_{late}$) indicates a cognitive process related to the extraction of information relevant to successful execution of the task [Gaeta et al., 2003].

Another view would be to consider the latency and amplitude of the $P3_{late}$ bear some resemblance to the so-called P6 component. Indeed, such a component peaking around 500-600 msec was reported to be related to rule violation in a numerical task [Nunez-Pena and Honrubia-Serrano 2004]. Coherently, during INT, subjects had to manage the number/length interference as a perceptual violation of the "length equals number" rule.

Note that both views of our $P3_{late}$ are in line with the current debate about the P6 / $P3_{late}$ dissociation or association, since these components have very similar characteristics [Munte et al., 1998; Osterhout et al., 1996].

In summary, our ERP data fit very well with our behavioral data (RTs and error rates) showing that INT was a task that required a specific cognitive inhibition by adults.

fMRI data

The conjunction analysis of the fRMI data shed light on the areas activated in both conditions (INT and COV). The ventral pathway areas (from V1 to V4) were likely to reflect the identification of the visual stimulations (colored shapes) common to both conditions [Gulyas et al., 1994; Zeki et al., 1991]. In the right hemisphere, we also observed activation of the occipito-temporal junction, which is known to be involved in visual discrimination of forms spatially presented in a row display [Vidnyanszky et al., 2000]. In the present study, this mechanism was indispensable for numerical quantification, i.e. the decomposition of the rows of forms (squares or rectangles) into discrete units. The dorsal pathway areas were likely to reflect visuospatial information processing [Haxby et al., 1991], here corresponding to the exploration of the computer screen that was divided into two spaces by a horizontal line. More precisely, the bilateral

superior parietal cortices are known to be involved in attentional processes [Corbetta et al., 1998; Corbetta et al., 1993; Petit et al., 1996], whereas the bilateral inferior parietal cortices were more specifically activated in numerical processes, as for number comparison [Chochon et al., 1999] or subitizing [Piazza et al., 2002], which fit both experimental conditions well. We also know that the inferior parietal cortex is activated during complex calculations [Zago et al., 2001].

The conjunction analysis also brought a set of right frontal areas to light. On the external surface, we observed the middle frontal gyrus activation known to be involved in object and spatial working memory [Owen 1997] and which probably corresponded here to the required mental manipulation necessary for the numerical comparison. We also observed the activation of the opercular part of the inferior frontal gyrus, which was likely to reflect a form of spontaneous episodic memory retrieval [Herrmann et al., 2001], that is, the retrieval of visuospatial configurations (the repeated row displays) during task monitoring.

Concerning the overall condition effect, the right occipital cortex, which is known to be involved in visuospatial vigilance and attention [Martinez et al., 1999; Mesulam 2000; Murray and Wojciulik 2004; Pardo et al., 1991; Petit et al., 1999], particularly during numerical tasks such as subitizing and counting [Piazza et al., 2002], was more activated in INT than in COV. Here, it appeared to be specifically recruited by cognitive inhibition of number/length interference during the Piaget-like task [Houdé and Guichart 2001]. Our data show that in a numerical task with visuospatial stimulus, executive attention (inhibitory control) is implemented in posterior unimodal brain areas [Mesulam 2000], while in other logico-mathematical tasks such as reasoning with linguistic rules, executive attention is implemented in heteromodal prefrontal areas [Houdé 2000; Houdé and Tzourio-Mazoyer 2003; Houdé et al., 2001]. Consequently, it does not seem that a

modality- and task-independent, unique “cognitive-inhibition center” exists in the human brain. This neuroimaging insight fits well with data from developmental psychology [Houdé 2000] indicating that the processes of selection-inhibition are age- and domain-specific (for object construction, number, categorization, and reasoning). It is also consistent with the recent idea that high-order cognition, such as the representation and use of conceptual knowledge, may be implemented in modality-specific systems [Barsalou et al., 2003].

Interestingly, the highest activation of the posterior part of the left inferior temporal gyrus in INT was likely to reflect the enhanced visual computing (linked to subitizing or counting) of objects (the colored squares) [Mazard et al., 2005] required to avoid the spatial "trap" triggered off by the two unequal rows.

One should also note that a set of left-lateralized frontal and temporal regions was deactivated in INT and activated in COV. Other authors have already reported such a deactivation of left frontal areas during numerical tasks [Zago et al., 2001]. Here we can suppose that it was here an inter-hemispheric balance phenomenon [Tzourio-Mazoyer et al., 2004], since the right visuospatial areas were particularly enhanced for executive attention in INT (see above). The deactivation of the left SMG, known to be involved in number-language interactions [Houdé and Tzourio-Mazoyer 2003; Zago et al., 2001], may be understood in the same vein.

Finally, concerning the block response shape, we noticed a greater activation in INT than in COV in the left inferior occipital cortex. As this region is contiguous with the posterior part of the left inferior temporal gyrus, its greater activation in INT than in COV is also likely to reflect the enhanced visual computing that occurs during inhibitory control. The other regions were also observed in the conjunction analysis, but they appeared here

with a greater activation at the end of the block in INT than in COV, which was likely to reflect the sustained attentional effort needed to inhibit number/length interference.

Finally, we attempt to integrate both the ERP and fMRI results. They are congruent with regard to the P3 component. Greater amplitude was found in COV than in INT. Some authors have already reported P3 generator localizations in the lateral prefrontal cortex, the cortico-limbic circuits, and the cingulates [Knight 1996; Knight and Scabini 1998; Soltani and Knight 2000]. This is consistent with the fMRI results (see Fig. 7) since the identification of most of these regions was found to be significant based on COV *minus* INT contrast.

Our ERP contour maps showed a frontal N2 component. Some authors have reported N2 generator localizations in the medial frontal regions, the right inferior frontal gyrus, and the right ventral and dorsolateral frontal cortex [Bekker et al., 2005; Jackson et al., 1999; Lavric et al., 2004; Nieuwenhuis et al., 2003]. However, in our fMRI results, the direct INT *minus* COV comparison did not indicate significant differences in those frontal areas.

A first view is to consider that in the present fMRI results, the frontal regions mentioned above were activated in the conjunction of both conditions, with most of the right frontal areas more activated in INT than in COV. The N2 amplitude difference (INT greater than COV) might involve a weak frontal metabolic cost which was not detectable because the fMRI was insufficiently sensitive, an idea already reported by other authors [Linden et al., 1999; McCarthy et al., 1997].

Another view is to consider our paradigm very sensitive to habituation/automation, which induced a front-to-back shift (see Fig. 6) from the first session (EEG) to the second one (fMRI). It is consistent with the recent idea that high-order cognition such as the representation and use of conceptual knowledge may also be implemented in posterior modality-specific systems [Barsalou et al., 2003].

In conclusion, we provided the first attempt to image cognitive inhibition in a Piaget-like task in adults, with hemodynamic data. In order to integrate both results, it would be interesting to consider the same tasks in a simultaneous EEG-fMRI study, in future research.

Acknowledgements

We would like to thank Guy Perchey for his help in the subjects' recruitment. We are also grateful to Antoine Ducorps and Denis Schwartz for their technical assistance in the ERP acquisition, Franck Lamberton and Nicolas Delcroix for their help with the fMRI acquisition.

- 22 -

Table I. Grand average latency (msec) and amplitude (µV) of each ERP component, in the covariation (COV) and interference (INT) conditions. Statistics on condition and electrode effects are given.

	Condition effect			**Electrode effect**
	COV	**INT**	**F value**	**F value**
N1 amplitude	-6.1 ± 1.8	-5.6 ± 1.8	F(1,9)=2.3	F(28,252)=5.8***
N2 amplitude	2.2 ± 3.2	0.9 ± 2.6	F(1,9)=7.8*	F(32,288)=5.5**
$P3_{early}$ amplitude	7.6 ± 3.6	3.6 ± 2.5	F(1,9)=60.4***	F(49,441)=9.8**
$P3_{late}$ amplitude	-	2.6 ± 1.8	-	F(49,441)=14.2***
N1 latency	146 ± 70	149 ± 70	F(1,9)=1.9	F(28,252)=0.7
N2 latency	260 ± 23	277 ± 21	F(1,9)=17.6**	F(32,288)=1.0
$P3_{early}$ latency	359 ± 16	369 ± 20	F(1,9)=3.1	F(49,441)=1.2
$P3_{late}$ latency	-	556 ± 24	-	F(49,441)=0.9

Condition values are mean ± SD. * $P < 0.05$ ** $P < 0.01$ *** $P < 0.001$. Electrode P values are adjusted by the Greenhouse-Geisser correction.

- 23 -

Table II. AROIs (Anatomical Regions Of Interest): statistical analysis. For each hemisphere, the left column shows AROIs found to be conjointly significant in the COV and INT conditions (labeled "Conjunction"). The right column shows the ANOVA results, with the overall condition effect and the Cond x HRL interaction. COV, covariance condition; INT, interference condition; Cond, overall condition effect; HRL, hemodynamic response latency.

	Left Hemisphere			Right Hemisphere		
	Conjunction	ANOVA		Conjunction	ANOVA	
Occipital lobe	COV / INT	Cond	Cond x HRL	COV / INT	Cond	Cond x HRL
Calcarine fissure and surrounding cortex	*** / ***			*** / ***		
Cuneus	** / **		**	*** / ***		**
Fusiform gyrus	*** / ***			*** / ***		
Lingual gyrus	*** / ***		*	*** / ***		
Superior occipital gyrus	*** / ***		*	*** / ***	*	
Middle occipital gyrus	*** / ***			*** / ***	*	
Inferior occipital gyrus	** / ***		*	** / **		
Temporal lobe						
Middle temporal gyrus		*			**	**
Inferior temporal gyrus		*		*** / ***		*
Parietal lobe						
Superior parietal gyrus	*** / ***		*	*** / ***		
Inferior parietal gyrus	*** / **			*** / ***		
Supramarginalis gyrus		*	***			*
Frontal lobe						
Superior frontal gyrus		***				
Middle frontal gyrus		*		** / *		
Inferior frontal gyrus, orbital part		*				
Inferior frontal gyrus, opercular part				*** / ***		
Superior frontal gyrus, medial part		**			**	
Limbic lobe						
Anterior cingulate and paracingulate gyri		*			*	
Median cingulate and paracingulate gyri		*			*	

* P < 0.05 ** P < 0.01 *** P < 0.001

- 24 -

References

Ashburner J, Friston KJ. (1999): Nonlinear spatial normalization using basis functions. J Acoust Soc Am 106:449-57.

Barsalou LW, Kyle Simmons W, Barbey AK, Wilson CD. (2003): Grounding conceptual knowledge in modality-specific systems. Trends Cogn Sci 7:84-91.

Bekker EM, Kenemans JL, Verbaten MN. (2005): Source analysis of the N2 in a cued Go/NoGo task. Brain Res Cogn Brain Res 22:221-31.

Bruin KJ, Wijers AA, van Staveren AS. (2001): Response priming in a go/NoGo task: do we have to explain the go/NoGo N2 effect in terms of response activation instead of inhibition? Clin Neurophysiol 112:1660-71.

Bush G, Luu P, Posner MI. (2000): Cognitive and emotional influences in anterior cingulate cortex. Trends Cogn Sci 4:215-222.

Bush G, Vogt BA, Holmes J, Dale AM, Greve D, Jenike MA, Rosen BR. (2002): Dorsal anterior cingulate cortex: a role in reward-based decision making. Proc Natl Acad Sci U S A 99:523-8.

Chochon F, Cohen L, van de Moortele PF, Dehaene S. (1999): Differential contributions of the left and right inferior parietal lobules to number processing. J Cogn Neurosci 11:617-30.

Collins DL, Neelin P, Peters TM, Evans AC. (1994): Automatic 3D Intersubject Registration of MR Volumetric Data in Standardized Talairach Space. Journal of Computer Assisted Tomography 18:192-205.

Comerchero MD, Polich J. (1998): P3a, perceptual distinctiveness, and stimulus modality. Brain Res Cogn Brain Res 7:41-8.

Comerchero MD, Polich J. (1999): P3a and P3b from typical auditory and visual stimuli. Clin Neurophysiol 110:24-30.

Corbetta M, Akbudak E, Conturo TE, Drury HA, Linenweber MR, Ollinger JM, Petersen SE, Raichle ME, Snyder AZ, Van Essen DC and others. (1998): A common cortical network for attention and eye movements. Neuron 21:761-768.

Corbetta M, Miezin FM, Shulman GL, Petersen SE. (1993): A PET study of visuospatial attention. J.Neurosci. 13:1202-1226.

Daurignac E, Houdé O, Jouvent R. (2005): Negative priming in a numerical Piaget-like task in adults as evidenced by ERP. J Cogn Neurosci (in press).

Delorme A, Makeig S. (2004): EEGLAB: an open source toolbox for analysis of single-trial EEG dynamics including independent component analysis. J Neurosci Methods 134:9-21.

Dempster FN. 1995. Interference and Inhibition in Cognition. In: Dempster FN, Brainerd CJ, editors. Interference and Inhibition in Cognition. New-York: Academic Press. p 3-26.

Diamond A. 1991. Neuropsychological insights into the meaning of object concept development. In: Carey S, Gelman R, editors. The epigenesis of mind: Essays on biology and cognition: Hillsdale: Lawrence Erlbaum. p 67-110.

Diamond A, Kirkham N, Amso D. (2002): Conditions under which young children can hold two rules in mind and inhibit a prepotent response. Developmental Psychology 38:352-362.

Eimer M. (1993): Effects of attention and stimulus probability on ERPs in a Go/NoGo task. Biol Psychol 35:123-38.

Falkenstein M, Hoormann J, Hohnsbein J. (1999): ERP components in Go/NoGo tasks and their relation to inhibition. Acta Psychol (Amst) 101:267-91.

Falkenstein M, Koshlykova NA, Kiroj VN, Hoormann J, Hohnsbein J. (1995): Late ERP components in visual and auditory Go/NoGo tasks. Electroencephalogr Clin Neurophysiol 96:36-43.

Friston K, Ashburner J, Poline JB, Frith CD, JD H, RSJ F. (1995): Spatial registration and normalization of images. *Human Brain mapping* 2:165-189.

Gaeta H, Friedman D, Hunt G. (2003): Stimulus characteristics and task category dissociate the anterior and posterior aspects of the novelty P3. Psychophysiology 40:198-208.

Gulyas B, Heywood CA, Popplewell DA, Roland PE, Cowey A. (1994): Visual form discrimination from color or motion cues: Functional anatomy by positron emission tomography. Proc.Natl.Acad.Sci.USA 91:9965-9969.

Haxby JV, Grady CL, Horwitz B, Ungerleider LG, Mishkin M, Carson RE, Herscovitch P, Schapiro MB, Rapoport SI. (1991): Dissociation of object and spatial visual processing pathways in human extrastriate cortex. Proc.Natl.Acad.Sci.USA 88:1621-1625.

Herrmann M, Rotte M, Grubich C, Ebert AD, Schiltz K, Munte TF, Heinze HJ. (2001): Control of semantic interference in episodic memory retrieval is associated with an anterior cingulate-prefrontal activation pattern. Hum Brain Mapp 13:94-103.
Houdé O. (2000): Inhibition and cognitive development: object, number, categorization and reasoning. Cognitive development 15:63-73.
Houdé O. 2001. Interference and inhibition (Psychology of -). In: Inc PP, editor. International Encyclopedia of the Social and Behavioral Sciences: Oxford: Elsevier. p 7718-7722.
Houdé O, Guichart E. (2001): Negative priming effect after inhibition of number/length interference in a Piaget-like task. Developemental Science 4:119-123.
Houdé O, Tzourio-Mazoyer N. (2003): Neural foundations of logical and mathematical cognition. Nat Rev Neurosci 4:507-14.
Houdé O, Zago L, Crivello C, Moutier S, Pineau A, Mazoyer B, Tzourio N. (2001): Access to deductive logic depends on a right ventromedial prefrontal area devoted to emotion and feeling: evidence from a training paradigm. NeuroImage 14:1486-1492.
Houdé O, Zago L, Mellet E, Moutier S, Pineau A, Mazoyer B, Tzourio-Mazoyer N. (2000): Shifting from the perceptual brain to the logical brain: the neural impact of cognitive inhibition training. J Cogn Neurosci 12:721-8.
Hunter M, Turner A, Fulham WR. (2001): Visual signal detection measured by event-related potentials. Brain Cogn 46:342-56.
Jackson SR, Jackson GM, Roberts M. (1999): The selection and suppression of action: ERP correlates of executive control in humans. Neuroreport 10:861-5.
Jung TP, Makeig S, Humphries C, Lee TW, McKeown MJ, Iragui V, Sejnowski TJ. (2000): Removing electroencephalographic artifacts by blind source separation. Psychophysiology 37:163-78.
Katayama J, Polich J. (1998): Stimulus context determines P3a and P3b. Psychophysiology 35:23-33.
Keating DP. 2004. Cognitive and brain development. In: Lerner RJ, Steinberg L, Editors. Handbook of the Adolescent Psychology: Wiley. p 45-84.
Knight R. (1996): Contribution of human hippocampal region to novelty detection. Nature 383:256-9.
Knight RT, Scabini D. (1998): Anatomic bases of event-related potentials and their relationship to novelty detection in humans. J Clin Neurophysiol 15:3-13.
Kopp B, Mattler U, Goertz R, Rist F. (1996): N2, P3 and the lateralized readiness potential in a NoGo task involving selective response priming. Electroencephalogr Clin Neurophysiol 99:19-27.
Lavric A, Pizzagalli DA, Forstmeier S. (2004): When 'Go' and 'NoGo' are equally frequent: ERP components and cortical tomography. Eur J Neurosci 20:2483-8.
Linden DE, Prvulovic D, Formisano E, Vollinger M, Zanella FE, Goebel R, Dierks T. (1999): The functional neuroanatomy of target detection: an fMRI study of visual and auditory oddball tasks. Cereb Cortex 9:815-23.
Martinez A, Anllo-Vento L, Sereno MI, Frank LR, Buxton RB, Dubowitz DJ, Wong EC, Hinrichs H, Heinze HJ, Hillyard SA. (1999): Involvement of striate and extrastriate visual cortical areas in spatial attention. Nat Neurosci 2:364-9.
Mazard A, Joliot M, Mellet E. (2005): Impact of the semantic content on functional anatomy of visual mental imagery. Brain Research (In press).
McCarthy G, Luby M, Gore J, Goldman-Rakic P. (1997): Infrequent events transiently activate human prefrontal and parietal cortex as measured by functional MRI. J Neurophysiol 77:1630-4.
Mesulam MM. 2000. Right Hemispheric Dominance For Spatial Attention. In: Press OU, editor. Principles of Behavioral and Cognitive Neurology. Hardcover ed. New-York. p 213-218.
Munte TF, Heinze HJ, Matzke M, Wieringa BM, Johannes S. (1998): Brain potentials and syntactic violations revisited: no evidence for specificity of the syntactic positive shift. Neuropsychologia 36:217-26.
Murray SO, Wojciulik E. (2004): Attention increases neural selectivity in the human lateral occipital complex. Nat Neurosci 7:70-4.
Nieuwenhuis S, Yeung N, Cohen JD. (2004): Stimulus modality, perceptual overlap, and the go/no-go N2. Psychophysiology 41:157-60.
Nieuwenhuis S, Yeung N, van den Wildenberg W, Ridderinkhof KR. (2003): Electrophysiological correlates of anterior cingulate function in a go/no-go task: effects of response conflict and trial type frequency. Cogn Affect Behav Neurosci 3:17-26.

Nunez-Pena MI, Honrubia-Serrano ML. (2004): P600 related to rule violation in an arithmetic task. Brain Res Cogn Brain Res 18:130-41.
Oldfield RC. (1971): The assessment and analysis of handedness: the Edinburgh inventory. Neuropsychologia 9:97-113.
Osterhout L, McKinnnon R, Bersick M, Corey V. (1996): On the language specificity of the brain response to syntactic anomalies: is the syntactic positive shift a member of the P300 family? J Cogn Neurosci:507-526.
Owen AM. (1997): The functional organization of working memory processes within human lateral frontal cortex: the contribution of functional neuroimaging. Eur J Neurosci 9:1329-39.
Pardo JV, Fox PT, Raichle ME. (1991): Localization of a human system for sustained attention by positron emission tomography. Nature 349:61-64.
Paus T. (2005): Mapping brain maturation and cognitive development during adolescence. Trends Cogn Sci 9:60-8.
Petit L, Dubois S, Tzourio N, Dejardin S, Crivello F, Michel C, Etard O, Denise P, Roucoux A, Mazoyer B. (1999): A PET study of the human foveal fixation system. Human Brain Mapping 8:28-43.
Petit L, Orssaud C, Tzourio N, Crivello F, Berthoz A, Mazoyer B. (1996): Functional anatomy of a prelearned sequence of horizontal saccades in humans. The Journal of Neuroscience 16:3714-3726.
Piaget J. 1952. The child's conception of number. New York: Basic Books (original in French, 1941).
Piazza M, Mechelli A, Butterworth B, Price CJ. (2002): Are subitizing and counting implemented as separate or functionally overlapping processes? NeuroImage 15:435-46.
Polich J. 2003. Theorical overview of P3a and P3b. In: Polich J, editor. Detection of Change: Event-Related Potential and fMRI Findings. Kluwer Academic Press: Boston. p 83-98.
Polich J. (2004): Clinical application of the P300 event-related brain potential. Phys Med Rehabil Clin N Am 15:133-61.
Polich J, Comerchero MD. (2003): P3a from visual stimuli: typicality, task, and topography. Brain Topogr 15:141-52.
Posner MI, Rothbart MK. (1998): Attention, self-regulation and consciousness. Philos Trans R Soc Lond B Biol Sci 353:1915-27.
Soltani M, Knight RT. (2000): Neural origins of the P300. Crit Rev Neurobiol 14:199-224.
Steinberg L. (2005): Cognitive and affective development in adolescence. Trends Cogn Sci 9:69-74.
Tzourio-Mazoyer N, Josse G, Crivello C, Mazoyer B. (2004): Interindividuality variability in the hemispheric organization for speech. NeuroImage 21:422-435.
Tzourio-Mazoyer N, Landeau B, Papathanassiou D, Crivello C, Etard O, Delcroix N, Mazoyer B, Joliot M. (2002): Automated anatomical labelling of activations in SPM using a macroscopic anatomical parcellation of the MNI MRI single subject brain. NeuroImage 15:273-89.
Verard L, Allain P, Travere JM, Baron JC, Bloyet D. (1997): Fully automatic identification of AC and PC landmarks on brain MRI using scene analysis. IEEE Trans Med Imaging 16:610-6.
Vidnyanszky Z, Gulyas B, Roland PE. (2000): Visual exploration of form and position with identical stimuli: functional anatomy with PET. Hum Brain Mapp 11:104-16.
Woods RP, Cherry SR, Mazziotta JC. (1992): Rapid automated algorithm for aligning and reslicing PET images. Journal of Computer Assisted Tomography 16:620-633.
Zago L, Pesenti M, Mellet E, Crivello F, Mazoyer B, Tzourio-Mazoyer N. (2001): Neural correlates of simple and complex mental calculation. NeuroImage 13:314-27.
Zeki S, Watson JDG, Lueck CJ, Friston KJ, Kennard C, Frackowiak RSJ. (1991): A direct demonstration of functional specialization in human visual cortex. J. Neurosci. 11:641-649.

- 27 -

Figure legends

Figure 1. Experimental design. The subject had to judge the numerical equivalence of two rows displayed on a computer screen. They were instructed to respond by pressing the "same-number" button or the "not-the-same-number" button as quickly as possible, without making any error. In the first run, the number and the length covaried (COV), whereas in the second run, the participant had to inhibit (INT) the misleading strategy "length equals number".

Figure 2. Mean reaction times (RTs, top part) and error percentages (bottom part) for each session (EEG, fMRI) and condition (COV, INT). RTs and errors were artificially grouped into blocks of 8 items each. Circles: COV. Squares: INT.

Figure 3. Grand average ERP waveforms at midline electrodes for both conditions (COV and INT). For each condition and component (N1, N2, $P3_{early}$, and $P3_{late}$), the latencies were plotted at their maxima. Electrode sets are displayed on a schematic head (nose is up).

Figure 4. Grand average topographic maps of COV and INT voltages, at N1, N2, and P3 maxima.

Figure 5. Activated regions of the conjunction of COV and INT. L: left, R: Right. MNI coordinate space.

- 28 -

Figure 6. Regions more activated in INT than in COV.

Figure 7. Blue: Regions deactivated in INT and activated in COV. Yellow: Regions more activated in COV than in INT. L: left, R: Right. MNI coordinate space.

- 29 -

Figure 1.

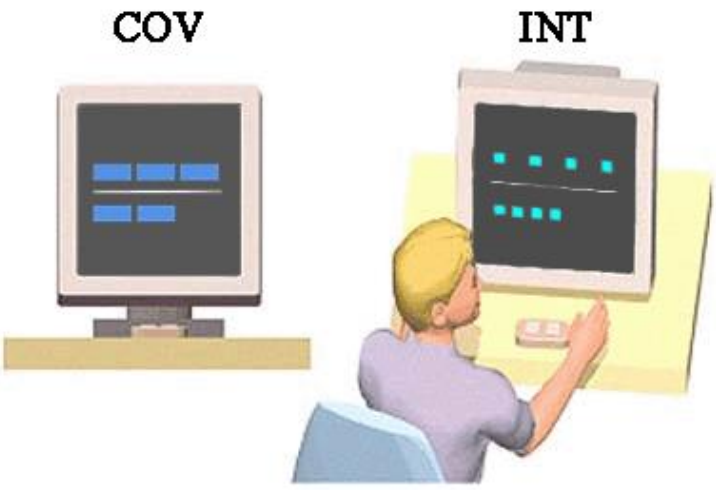

- 30 -

- 31 -

Figure 2.

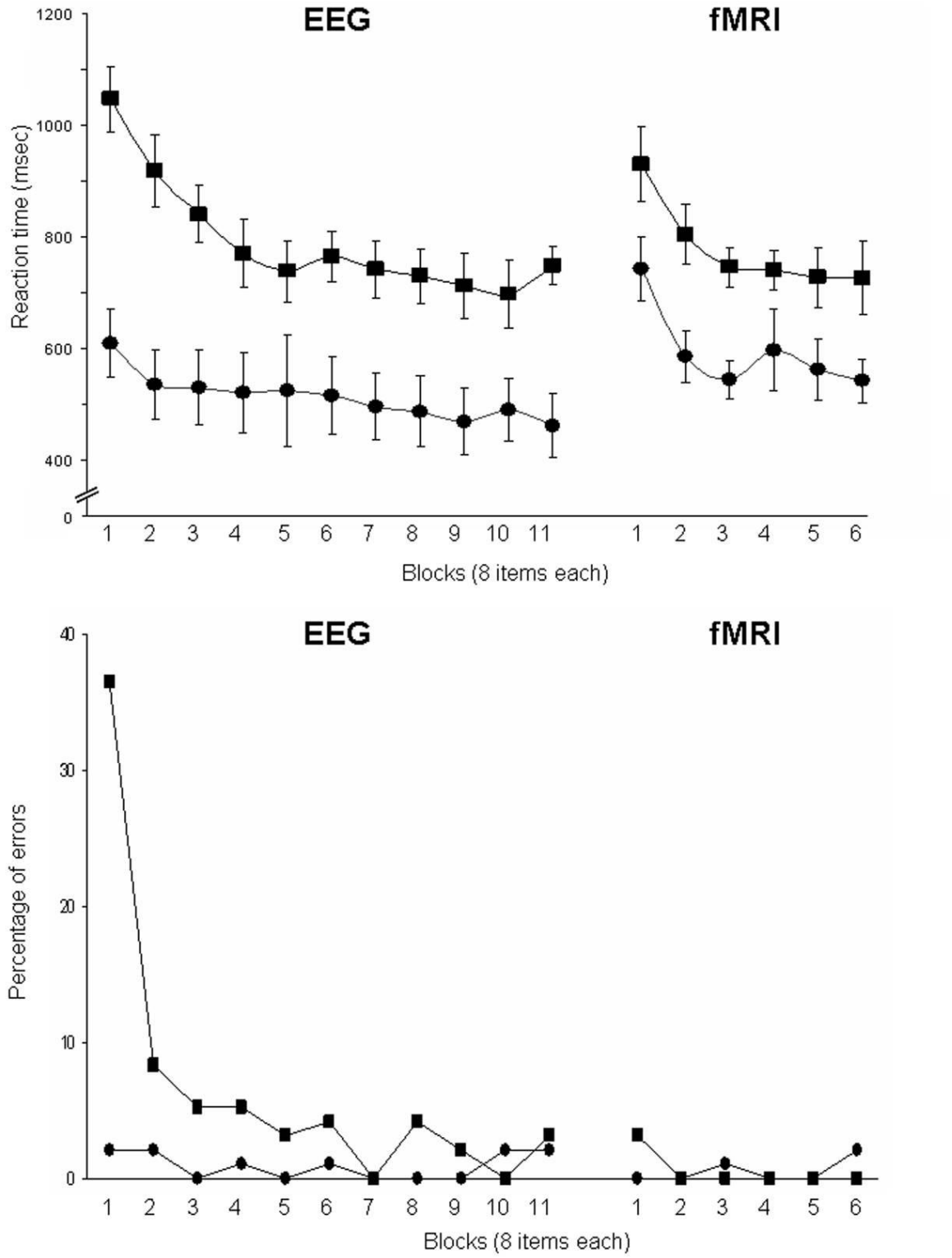
EEG
fMRI
Reaction time (msec)
1200
1000
800
600
400
0
1 2 3 4 5 6 7 8 9 10 11
1 2 3 4 5 6
Blocks (8 items each)
EEG
fMRI
Percentage of errors
40
30
20
10
0
1 2 3 4 5 6 7 8 9 10 11
1 2 3 4 5 6
Blocks (8 items each)

- 32 -

Figure 3.

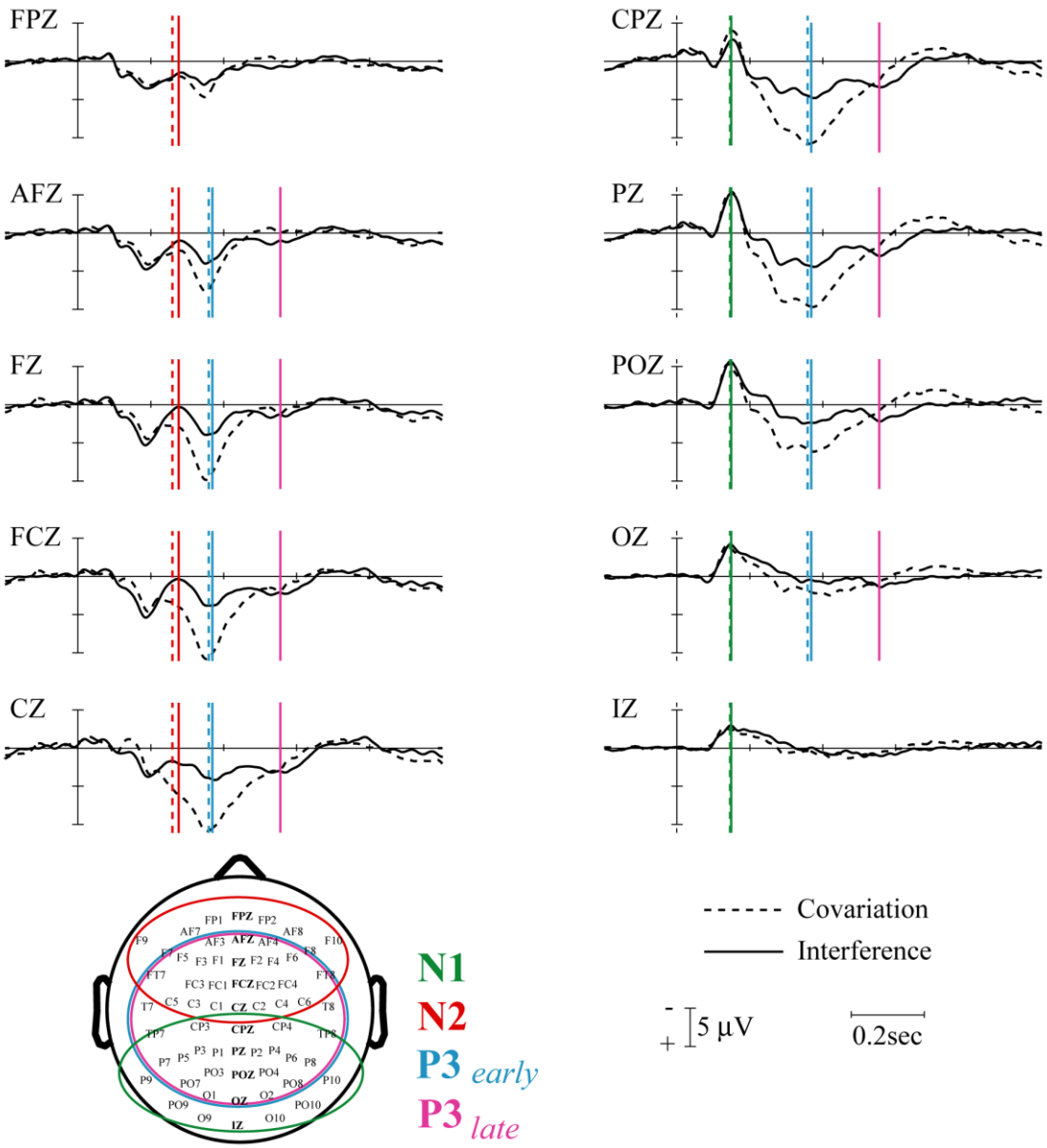
FPZ
CPZ
AFZ
PZ
FZ
POZ
FCZ
OZ
CZ
IZ
N1
N2
P3 early
P3 late
Covariation
Interference
5 µV
0.2sec

- 33 -

Figure 4.

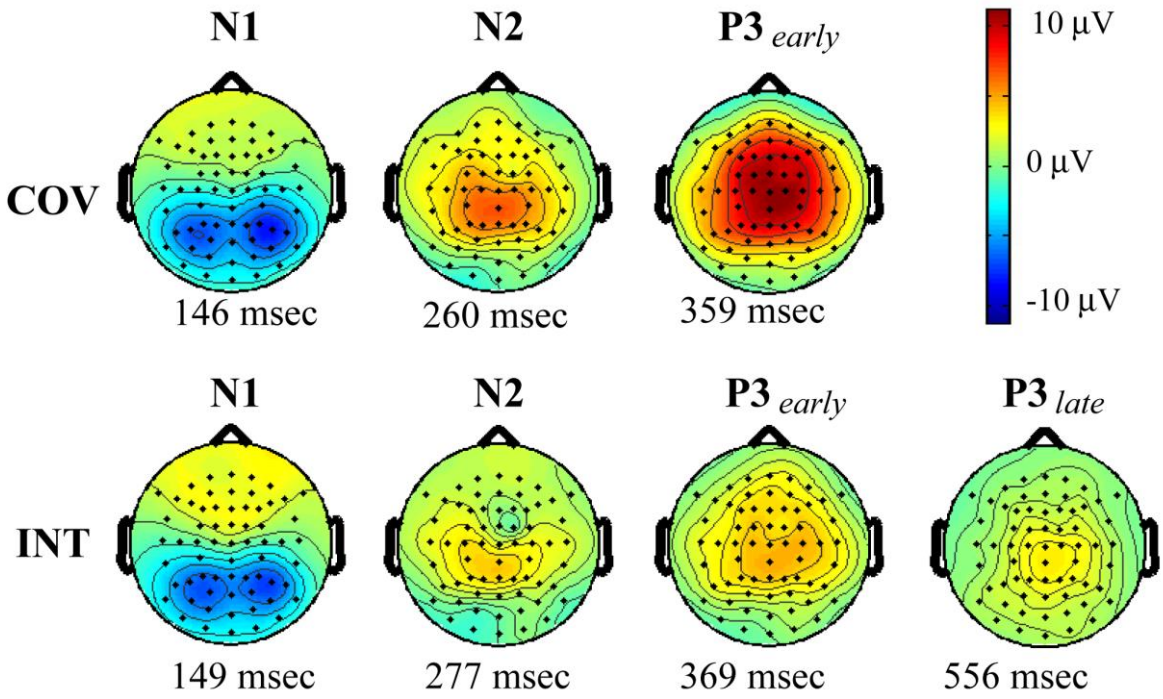
N1
N2
P3 early
10 µV
0 µV
-10 µV
COV
146 msec
260 msec
359 msec
N1
N2
P3 early
P3 late
INT
149 msec
277 msec
369 msec
556 msec

- 34 -

Figure 5.

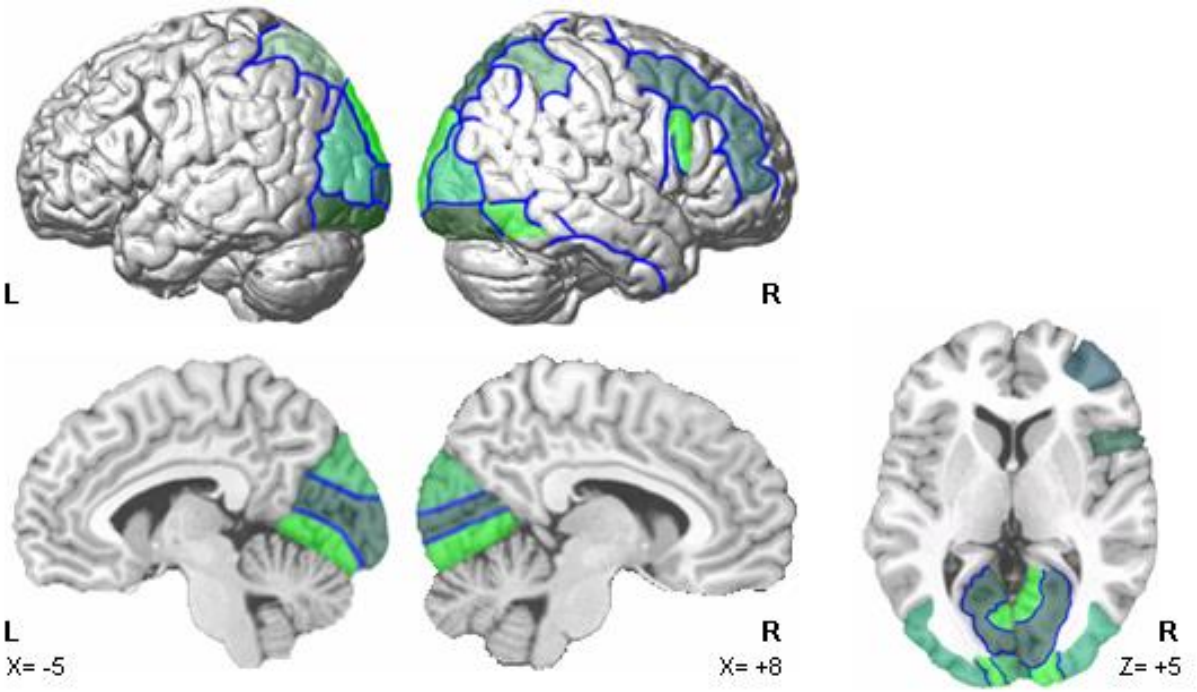

- 35 -

Figure 6.

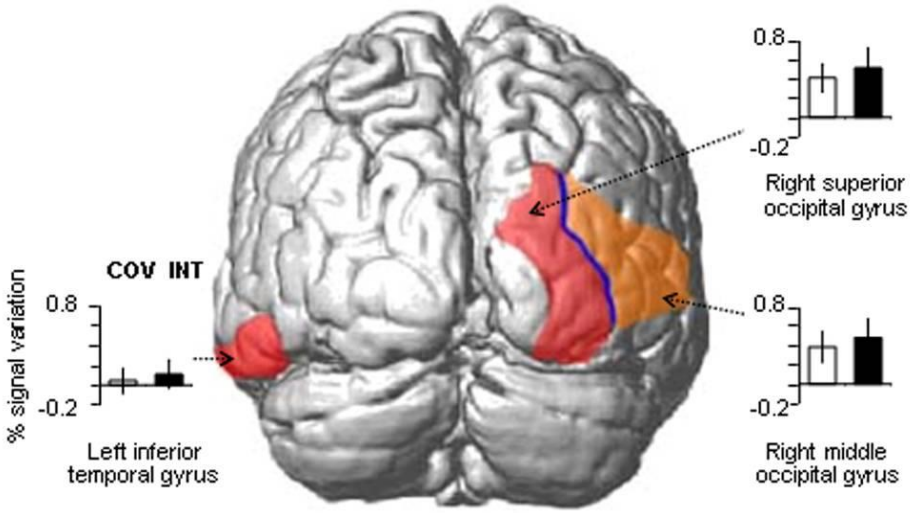
COV INT
% signal variation
0.8
-0.2
Left inferior
temporal gyrus
0.8
-0.2
Right superior
occipital gyrus
0.8
-0.2
Right middle
occipital gyrus

- 36 -

Figure 7.

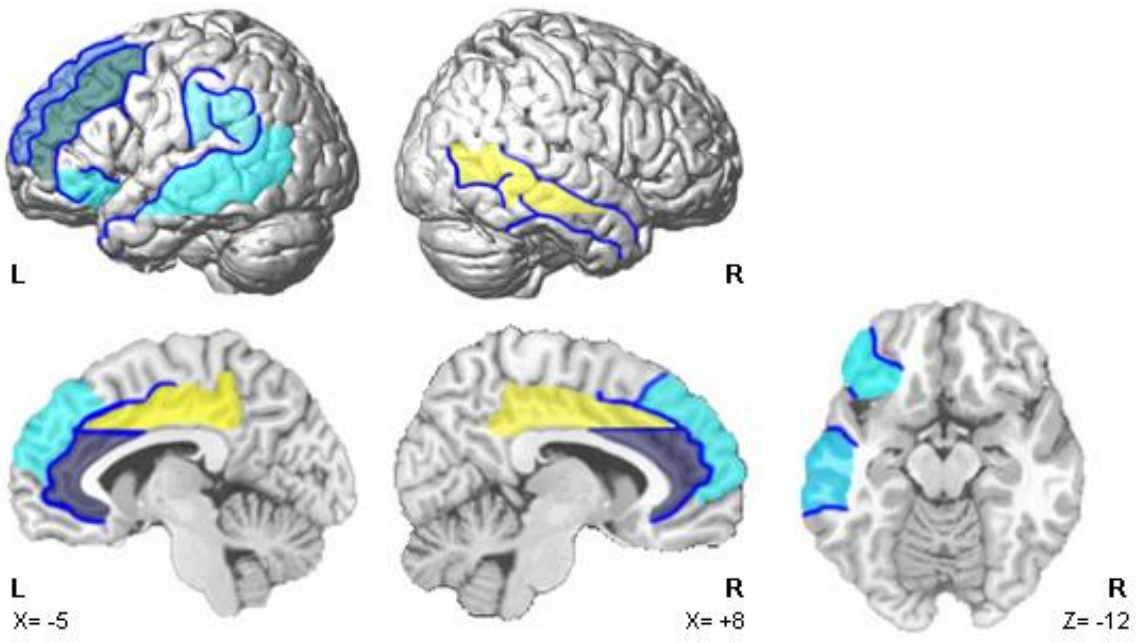

- 37 -